

Qualitative and quantitative changes in detrital reservoir rocks caused by CO₂-brine-rock interactions during first injection phases (Utrillas sandstones, Northern Spain)

E. Berrezueta¹ B. Ordóñez-Casado¹, L. Quintana^{2,1}

[1]{Instituto Geológico y Minero de España, Oviedo, Spain}

[2]{Departamento de Geología, Universidad de Oviedo, Spain}

Correspondence to: E. Berrezueta (e.berrezueta@igme.es)

Abstract

The aim of this article is to describe and interpret qualitative and quantitative changes at rock matrix scale of Lower-Upper Cretaceous sandstones exposed to supercritical (SC) CO₂ and brine. The effects of experimental injection of SC CO₂ during the first injection phases were studied at rock matrix scale, in a potential deep sedimentary reservoir in Northern Spain (Utrillas unit, at the base of the Cenozoic Duero Basin).

Experimental wet CO₂ injection was performed in a reactor chamber under realistic conditions of deep saline formations ($P \approx 7.8$ MPa, $T \approx 38$ °C and 24 h exposure time). After the experiment, exposed and non-exposed equivalent sample sets were compared with the aim of assessing possible changes due to the effect of the CO₂-brine exposure. Optical microscopy (OpM) and scanning electron microscopy (SEM) aided by optical image analysis (OIA) were used to compare the rock samples and get qualitative and quantitative information about mineralogy, texture and porous network distribution. Chemical analyses were performed to refine the mineralogical information and to obtain whole rock geochemical data. Brine composition was also analysed before and after the experiment.

The results indicate an evolution of the pore network (porosity increase $\approx 2\%$). Intergranular quartz matrix detachment and partial removal from the rock sample (due to CO₂ input/release dragging) are the main processes that may explain the porosity increase. Primary mineralogy ($\approx 95\%$ quartz) and rock texture (heterogeneous sand with interconnected framework of

1 micro-channels) are important factors that seem to enhance textural/mineralogical changes in
2 this heterogeneous system. The whole rock and brine chemical analyses after interaction with
3 SC CO₂-brine do not present important changes in the mineralogical, porosity and chemical
4 configuration of the rock with respect to initial conditions, ruling out relevant precipitation or
5 dissolution at these early stages.

6 These results, simulating the CO₂ injection near the injection well during the first phases (24
7 h) indicate that, in this environment where CO₂ displaces the brine, the mixture principally
8 generates local mineralogical/textural re-adjustments due to physical detachment of quartz
9 grains.

10 Consequences deriving from these changes are variable. Possible porosity and permeability
11 increases could facilitate further CO₂ injection but textural re-adjustment could also affect the
12 rock physically. However, it is not clear yet what effect the quartz (solid suspension) could
13 provoke in more distant areas of the rock. Quartz could be transported in the fluid flow path
14 and probably accumulated at pore throats.

15 **Key Word:** CO₂ storage, Utrillas sandstones, applied petrology, pore changes.

16

17 **1 Introduction and objectives**

18 The capture and geological sequestration of CO₂ is one of the technological options currently
19 contemplated to reduce emissions of greenhouse gases into the atmosphere. Deep geological
20 storage in porous rock formations is considered the most appropriate strategy for CO₂
21 sequestration (Bachu, 2000; Izgec et al., 2008; Benson and Cole, 2008; Gaus, 2010) and
22 injectivity is a key technical and economic issue for carbon capture and storage (CCS)
23 projects (Bacci et al., 2011). The viability of the CO₂ injection depends mainly on the porosity
24 and permeability of reservoir rocks. CO₂ interaction with the host rock, such as dissolution or
25 precipitation of minerals is also important (e.g. Ross et al., 1982; Sayegh et al.; 1990 and
26 Saeedi et al., 2011), as well as mineral trapping (Kaszuba et al., 2003; Rosenbauer et al.,
27 2005; Liu et al., 2013). Dissolution of supercritical (SC) CO₂ into brine will control the rate of
28 dissolution and precipitation of minerals constituting the porous rock. Volume changes of the
29 solid phase will modify the pore structure, affecting both porosity and permeability of the
30 porous media (André et al., 2007).

1 CO₂-water-rock interaction experiments represent a useful method to understand and explore
2 the mechanisms and processes of geological storage (Ketzer et al., 2009) and to design safe
3 underground CO₂ storage operations. Bertier et al. (2006) built an experimental setup to
4 evaluate the effect of CO₂-water-rock interactions in three sandstone aquifers concluding that
5 “CO₂-water-rock interactions might significantly influence geological sequestration of CO₂”.
6 Most of the experimental and theoretical studies are designed to simulate the injection of CO₂,
7 mixed with brine, into rocks at P-T conditions of deep storage environments. The result of
8 many of these experiments was an increase in the porosity/permeability of the reservoir rock
9 caused by partial dissolution of the carbonate components (mainly calcite) (Perkins and
10 Gunter, 1995; Svec and Grigg, 2001; Rochelle et al., 2004; Egermann et al., 2005; Izgec et al.,
11 2005; Gunter et al., 2004, Luquot and Gouze, 2009 and Desbois et al., 2011). However, other
12 set of experiments has shown porosity decreases due to the initial dissolution of carbonates
13 followed by secondary precipitation/mineralisation (Kaszuba et al., 2003; Cailly et al., 2005;
14 Kaszuba et al., 2005; Mito et al., 2008; Sterpenich et al., 2009; Luquot and Gouze, 2009).
15 André et al. (2007) presented numerical modelling of chemical fluid-rock interactions at the
16 SC-CO₂-liquid interface during CO₂ injection into a carbonate reservoir (Paris Basin, France).
17 In this case, two CO₂ injection scenarios were evaluated: CO₂-saturated water injection and
18 pure supercritical CO₂ injection. In these two scenarios, different geochemical processes
19 occurred as the distance from the injection well increased (in the first scenario there was a
20 porosity increase of up to 90%; while, in the second scenario porosity increased about 6% in
21 most of the reservoir and it decreased in the vicinity of the injection point). Besides, different
22 regions were identified depending on the saturation ranges of liquid and gas phases,
23 associated geochemical conditions and porosity variations during the injection and according
24 to the distance from the injection well (Fig. 1a).

25 Other investigations focus on the CO₂ injection into potential reservoir rock formations under
26 dry conditions (Kaszuba et al., 2003; Vickerd et al., 2006 and Berrezueta et al., 2013). The
27 injection environment is mainly envisaged as injecting CO₂ mixed with brine into sandstones.
28 However, in near-well conditions, the supercritical CO₂ laterally displaces the brine and
29 occupies the pore space of the rocks, in either dry or near-dry conditions (André et al., 2007;
30 Burton et al., 2008; Luquot and Gouze, 2009; Gaus, 2010). Therefore, dry CO₂ interaction
31 with the storage rock is a realistic scenario that takes place during the initial injection stages.
32 Some theoretical studies (Gaus et al., 2008 and Gaus, 2010) and experimental results
33 (Stepernich et al., 2009) on dry CO₂-rock interactions indicate the absence of reactions and

1 consequently negligible textural-mineralogical changes. This is explained by the lack of H₂O
2 in the system that prevents dissolution/precipitation and any kind of chemical reactions.
3 However, experimental studies on dry-CO₂ injection into undersaturated sandstones with high
4 clay matrix content (Berrezueta et al., 2013) concluded in an increase of rock porosity,
5 causing a textural change. This was explained by detachment and partial removal of the
6 intergranular clay matrix from the sandstone samples due to supercritical CO₂ input/release
7 dragging and changes in electrical-polarity forces.

8 Our research is focussed on experimental injection of supercritical CO₂ into the selected rocks
9 (sandstones saturated by and covered with brine), similarly to previous works e.g. Tarkowski
10 and Wdowin (2011), Fischer et al. (2013), Wdowin et al., (2014a, b) and Tarkowski et al.,
11 (2015). We chose the Utrillas sandstones for the present study due to their importance as
12 potential CO₂ reservoirs in Spain. The lithological characteristics of the Utrillas sandstones
13 and the structural features of the area offer favourable conditions for the study of CO₂ storage
14 (García Lobón et al. 2010 and Martínez et al., 2013).

15 The selected P-T conditions and run-times of our experiments aim to reproduce the reservoir
16 rock dry-wet environment, adjacent to a theoretical injection borehole, (Fig. 1a and b),
17 specifically, at the interface between the supercritical CO₂ bubble and the aqueous solution.
18 This interface acts as an exchange zone where CO₂ diffuses constantly (e.g. Zone 4 defined by
19 André et al., 2007). The experimental P-T conditions were selected to guarantee that the CO₂
20 was over its supercritical point (Holloway 1997; Bachu 2000; Lake 1989; Span and Wagner
21 1996).

22 Furthermore, the textural-mineralogical and petrophysical changes in the rock samples are
23 studied before and after the experimental injection of supercritical CO₂ for a short period of
24 time (24 hours). Special care was put into the development of a model to explain the observed
25 changes. Optical image analysis (OIA) techniques were used to monitor these changes.

26

27 **2 Samples: geological setting**

28 The studied samples belong to the unit commonly known as Utrillas sandstones and locally
29 defined as Voznuevo Formation (Evers, 1967) of Upper Albian-Lower Cenomanian age
30 (Lower-Upper Cretaceous transition). The sampling took place in North Spain, at the
31 boundary between the Alpine Cantabrian Mountains and the Cenozoic Duero Basin (Fig. 2a).

1 The Utrillas sandstones belong to a 1100 m thick Cretaceous sequence and crop out near
2 Boñar village in North León province. This Cretaceous sequence lays unconformably on the
3 Paleozoic basement of the Variscan Cantabrian Zone. On top of the Cretaceous sequence, a
4 succession of almost 2500 m thick Cenozoic materials was deposited in the Duero Basin (Fig.
5 2d). The Cretaceous sequence has been divided into three parts (Manjón Rubio et al., 1982a):
6 1) a lower detrital part, which corresponds to the Utrillas sandstones, of continental origin;
7 2) an intermediate or transitional part of Turonian-Santonian age; and 3) an upper carbonate
8 part with limestones and marls of Santonian-Campanian age and marine origin (Fig. 2c). This
9 Cretaceous sequence was deposited in a post-rift stage, at the end of the Cretaceous
10 extensional phase that affected North Spain and produced the opening of the Bay of Biscay
11 (e.g. Gallastegui, 2000).

12 The Utrillas sandstones, in the study area, are composed of detrital, poorly consolidated or
13 unconsolidated whitish materials ranging from sandstone to conglomerate, with a maximum
14 size of pebbles of 6 cm. The succession is fining upwards with dominating conglomerates at
15 the base and progressively increasing sandstone ratio. The pebbles and grains are mainly of
16 quartzite origin and of subrounded to subangular form, with a sandy and kaolinitic matrix.
17 Argillaceous levels, paleochannels and cross-stratification are frequent and lignites appear
18 locally. This succession was formed in a fluvial braided environment and with a source area
19 composed of acid, mainly granitic and metamorphic, rocks. The transformation from feldspar
20 to kaolin occurred after the deposition and was the result of meteorization processes (Manjón
21 Rubio et al., 1982a).

22 The fluvial environment, in which the Utrillas sandstones were formed, represents the
23 proximal part of the Upper Cretaceous North-Iberian paleomargin. Towards the north, this
24 fluvial facies changed into deltaic facies, then talus facies and, finally, deep basin turbiditic
25 facies (Olive Davó et al., 1989). This paleomargin was deformed during the collision between
26 Iberia and Eurasia in Cenozoic times. This compressional event produced the uplift of the
27 Cantabrian Mountains in North Spain and the development of the Duero foreland basin in the
28 frontal part of the range (Alonso et al., 1996). The structure of the sampling area is relatively
29 simple and is characterized by a great monocline (Fig. 2d), the formation of which has been
30 related with a south-directed basement thrust inclined to the north (Alonso et al., 1996). In
31 detail the structure is more complex because the inclined limb of the monocline is disrupted

1 by an important fault, known as the Sabero Fault (Sabero-Gordón line of Rupke, 1965), that
2 produces the duplication of the Cretaceous sequence (Figs. 2b and d).

3 The Utrillas sandstone was sampled in three places of the complex inclined limb of the
4 monocline, in the area of Devesa of Boñar, performing a thorough study of the structure of
5 these target rocks and their seals (Figs. 2b, d and e). The sampling areas “Devesa 1” and
6 “Devesa 2” are located south of the Sabero Fault, in an outcrop of Cretaceous succession
7 dipping 80° towards the south. The sampling area “Devesa 3” is located north of the Sabero
8 Fault in an outcrop dipping 45° also southwards (Figs. 2b and d). For this study, we chose the
9 more consolidated sandstones (3 samples), located in “Devesa 1”, to guarantee the
10 effectiveness of the analysis. The unconsolidated sandstones of Devesa 2 and 3 were
11 discarded for the study. The samples were divided into adjoining and numbered sets of
12 blocks. Each couple of adjoining blocks was used for the experimental test and for the studies
13 before and after CO₂ injection.

14

15 **3 Methodology and experimental procedure**

16 **3.1 Experimental setup and procedure**

17 The experimental setup employed in this experiment (Fig. 1b) is based on similar systems
18 described by Luquot and Gouze (2009), Tarkowski and Wdowin (2011), Luquot et al. (2012),
19 Berrezueta et al. (2013) and Wdowin et al. (2014a, b). However, some modifications were
20 made due to the distinct characteristics of the target rock system. Sample material (rock type
21 and representative sample size), geological environment (pressure, temperature and salinity)
22 and technical equipment (materials for camera, software, pumps, etc.) were all considered for
23 the final arrangement of the experimental device and run conditions. The experiment consists
24 of the exposure of sandstones to SC CO₂ in a reactor with pressure and temperature control.
25 P/T conditions (7.8 MPa and 38° C, respectively) were selected to surpass the CO₂
26 supercritical point (Lake 1989; Span and Wagner 1996) and to simulate basic conditions of
27 injection and storage of CO₂ (Holloway 1997; Bachu 2000). These conditions are
28 representative of a depth of approx. 800 m. The selected exposure time (24 h) is meant to
29 model the first stage of injection.

30 The system (Fig. 1b) has two CO₂ cylinders (standard commercial CO₂ at 4.5 MPa) that are
31 linked to the other elements of the system by steel connectors (diameter: 5 mm). The second

1 CO₂ cylinder is connected to a piston pump that operates with a flow of 0.01 g/s. When the
2 required pressure (7.8 MPa) decreases (due to possible leaks), this pump will inject CO₂ to
3 keep the pressure within the desired values. The piston pump needs a CO₂ initial pressure of 1
4 MPa in order to inject CO₂ into the Hastelloy steel chamber (3 dm³), thereby, the pressure
5 between the piston pump and the second CO₂ cylinder has to be decreased by a pressure
6 manometer from 4.5 to 1 MPa. The inside of the chamber is coated with
7 polytetrafluoroethylene (PTFE) to protect the material against corrosion. At the bottom of the
8 chamber, a calorimeter controls the internal temperature. The calorimeter and the pump are
9 linked to the chamber with pressure and temperature sensors and are connected to a computer.

10 The experiments began with the saturation of rock samples (6 cubes of 27 cm³ of each
11 sandstone sample) with natural brine. 0.6 dm³ brine was chemically stabilized with the
12 samples for the saturation. 0.3 dm³ of this brine was extracted and analysed before SC CO₂
13 injection. Then, the rock samples were introduced into the chamber together with the rest of
14 brine. The experimental runs comprised: a) a pressurized CO₂ injection (3 h); b) a pressurized
15 stabilization (24 h, no CO₂ flow inside the chamber) and c) CO₂ pressure release (3 h). The
16 CO₂ injection was performed using a constrained hyperbaric chamber-reactor where the dry
17 CO₂ was pumped at pressures and temperatures of 7.8 MPa and 38°C, respectively. The times
18 of filling and emptying the chamber with supercritical CO₂ were the same (3 h). This is the
19 time required to reach the target pressure and temperature values, from the initial ambient
20 conditions. The same time was used to get back to the ambient conditions at the end of the
21 experimental test. The applied software, HEL 5.1, allows the remote control of the system
22 (experimental conditions) through the development of specific macros (pressure, temperature,
23 time) in real time. All the experimental runs were carried out in the laboratories of the
24 Geological Survey of Spain (IGME) in Tres Cantos, Madrid.

25 **3.2 Methodology of study**

26 The aim of the study was to quantify the possible textural and porosity changes due to
27 experimental CO₂ injection. We began with a detailed petrographic study using optical
28 microscopy (OpM) to identify the major mineral and textural features. The characterization
29 was performed in neighbouring areas of the blocks by OpM (30 µm thin sections) and
30 scanning electron microscopy (SEM, rock samples). Although the thin sections and SEM
31 samples do not exactly correspond to the same sample surface, they are located very close (a
32 few mm) in the original source-sample. The aim of the detailed OpM study and quantification

1 of mineralogical and textural variability was to verify that any changes observed in the
2 experiments were due to the effects of CO₂ effect and not to possible original heterogeneity.
3 Furthermore, chemical analysis of the brine and whole rock before and after SC CO₂ injection
4 were performed, as well as microscopic studies of the residue that remained in the reactor
5 chamber after the experiment.

6 Simultaneously, a detailed study of the configuration of porous system was conducted by
7 combining observation by scanning electron microscopy with backscattered electrons (SEM)
8 and optical image analysis (OIA). This method allows the study of pore size distribution and
9 other porosity parameters (shape, specific surface of pore, etc.). Later, the same procedure
10 was followed for the study of the SC CO₂ exposed rocks. The OIA technique makes it
11 possible to identify, characterize and quantify mineral elements in images captured digitally
12 (Fig. 3) before and after SC CO₂-brine exposure. The general procedure for the automated
13 image analysis was developed adapting the procedures and algorithms described by
14 Berrezueta et al. (2015), in order to quantify the textural and porosity changes (area,
15 roughness of minerals/pore boundaries, fractal dimension, roundness of minerals/pores and
16 porosity) provoked by experimental CO₂ injection. Assessment of pore-network distribution
17 by optical transmitted light studies of thin sections requires distinction between mineral and
18 pore networks according to their optical characteristics. The segmentation of the porous
19 system was made by regions, applying the “thresholding” segmentation method (based on
20 threshold values to turn a raw image into a binary one, the pixels being partitioned according
21 to their intensity value). In this way, we can quantify the evolution of small changes in the
22 configuration of pore network. This work was carried out in the Oviedo IGME laboratory
23 using a Leica DM 6000 polarization microscope and an Image Pro Plus-7.0 software and
24 ProgRes digital camera for pore network study by OIA. SEM studies were performed using a
25 Hitachi TM3000 microscope with X-ray microanalysis equipment.

26 Additionally, rock samples were analysed by X-ray fluorescence (XRF) and X-ray diffraction
27 (XRD), and brine composition was determined by several methods (ion chromatography, ICP,
28 pH, conductivity measurements). The studies were developed in the facilities of IGME
29 laboratory-Tres Cantos and Oviedo University Laboratory.

30

1 4 Results

2 4.1 Mineralogical and petrographic characterization and OIA pore-network 3 quantification

4 4.1.1 Samples before SC CO₂ injection

5 The studied rock is a medium to very coarse-grained sandstone (grain size from 90-1600 μm,
6 with a mode of 250 μm) with areas of fine to medium grain sizes, showing unoriented and
7 slightly to highly variable porous structure. The pores, that are 80-500 μm (up to 1400 μm) in
8 size, constitute up to 8 to 15% of the rock volume, although there are special areas with
9 porosity up to 20%. The grains are from moderately to poorly sorted. There are zones with a
10 slight anisotropy defined by the presence of matrix rich bands. The grain skeleton (Fig. 4a, c
11 and e) consists of quartz (> 95%), very minor potassium feldspars (orthoclase) and a small
12 amount of micas (muscovite and chlorite). Accessory minerals (a total of 1-5%) are opaque
13 minerals, such as iron oxides and hydroxides (hematite and limonite), in the form of
14 aggregates of 40-100 μm in size, dispersed in the matrix or as cement. Other accessory
15 minerals are brown and green tourmalines and zircon. The rock is **composed mainly by grain
16 skeleton supported** with a small proportion of matrix (< 5%) composed mostly by quartz and
17 minor phyllosilicates of the mica and clay groups (muscovite and/or illite and/or kaolinite)
18 and opaque minerals. Locally, cement is present as a film coating iron oxides and sintaxial
19 quartz. According to the Folk (1974) and Pettijohn et al. (1987) classification, it is a quartz-
20 arenite (> 95% of quartz). Some areas have higher matrix concentration (>15%) classified as
21 fine-medium grained quartz-greywacke. The quartz grains are mostly monocrystalline with
22 important size variability. The grains have angular to subangular shapes, from high to low
23 sphericity and with sizes ranging from 90 to 1400 μm. Moreover very rounded grains of
24 polycrystalline quartz (fairly minor amount) appear sometimes with a Fe oxide coating. They
25 are of significant size (900-1900 μm). Grains with internal crystals of > 30 μm size are the
26 most common. On the other hand, there are some polycrystalline quartz grains with elongated
27 shapes and large dimensions up to 2800 μm. Sometimes the internal crystalline units of the
28 polycrystalline quartz grains show preferred orientations (meta-quartzite origin). The internal
29 units can be of sizes < 30 μm (chert) or up to 180-240 μm. The orthoclase feldspars are very
30 scarce, have rounded edges with sizes up to 1400 μm and show a significant degree of
31 alteration to iron oxides, phyllosilicates (illite and/or kaolinite) and chlorite.

1 The porous system reaches estimated visual proportions of 8 to 15%. Adapting Choquette and
2 Pray (1970) and Lucia (1999) porosity nomenclatures for carbonates, various pore types were
3 identified. “Vuggy” pore type, corresponding to highly spherical and rounded pores with sizes
4 around 50-90 μm are common. “Intercrystalline” type pores were also observed. These are
5 irregularly shaped around skeletal grains with very rounded edges, possibly a product of
6 matrix solution. They present elongated shapes and sizes ranging from 140-220 μm up to 300
7 μm . There are also incipient “cavernous” type pores, with elongated shapes, of sizes of ca. 80-
8 170, even 550 μm . In addition, there are “fracture” type pores. The sizes of these pores
9 generally reach 80-200 μm but there are some larger elongated caverns (ca. 1400 μm).
10 “Protected” porosity below some quartz grains (500 μm) was also observed. The
11 mineralogical and pore network distribution has been corroborated by SEM observation (Figs.
12 5a, c, and e).

13 The pore network quantification by OIA (Table 1) was carried out in three thin sections with
14 images acquired with a magnification of 10x. The porosity percentage estimated by this
15 method ranges from 6.49 to 18.18% with an average of $11.41 \pm 0.14\%$. The maximum and
16 minimum area of pore was 172100 μm^2 and 9.2 μm^2 , respectively. The average pore area
17 size was 168 μm^2 . Curves of relative and absolute distribution of number of pores versus pore
18 area ranges and diagrams of weighted area related to pore area classes are presented in Figs.
19 6a and c for the samples before SC CO₂ injection.

20 **4.1.2 Samples after SC CO₂ injection**

21 The studied rock is a medium to very coarse grained, poorly-sorted sandstone (particle size
22 from 300 μm to 1800 μm). It is slightly to highly porous with a porosity of 12 to 18% of the
23 rock volume and with pore size up to 2.5 mm. The grains vary from high to low spherical and
24 from subrounded to rounded shapes and it is noteworthy that the quartz grains have a high
25 degree of fracturing. The rock has scarce anisotropy, primarily defined by a band of higher
26 matrix concentration and opaque minerals (Fe oxides). The skeleton (Fig. 4b, d and f) consists
27 mostly of quartz grains (> 95%), scarce potassium feldspars (orthoclase) and small amounts
28 of mica (muscovite). Quartz grains show high degree of fracturing and are primarily
29 monocrystalline with high or low sphericity and rounded edges. Their sizes vary from 300 to
30 1800 μm . Sometimes they are of low sphericity with rounded edges or subangular shapes,
31 with sizes ranging from 240 to 1000 μm , even up to 2.4 mm. On the other hand,
32 polycrystalline quartz is present with internal crystal units < 30 μm , with elongated shapes,

1 rounded edges and grain sizes between 700-1400 μm . Other polycrystalline quartz grains are
2 rounded with sizes up to 1000-2400 μm with internal structural units $> 30 \mu\text{m}$. Orthoclase
3 feldspars are very rounded and quite spherical, with sizes up to 2.4 mm. They sometimes
4 show alteration containing Fe oxides and phyllosilicates (possibly illite and /or kaolinite).
5 Accessory minerals are opaque minerals (iron oxides associated to iron hydroxides). These
6 opaque minerals appear in the form of large grains surrounding the skeleton grains or as
7 smaller crystals scattered in the sandy-clay matrix or oriented at the edges of matrix rich
8 bands. Other accessory minerals are tourmaline and zircon. The matrix ($< 15\%$) is composed
9 mainly by quartz and a small amount of phyllosilicates (possibly illite and/ or kaolinite and/or
10 smectite) and iron oxides. Opaque minerals are Fe oxides and hydroxides (hematite and
11 limonite) that are often associated with phyllosilicates (kaolinite and/or illite and/or smectite)
12 and mica (possibly muscovite). Based on the modal content of quartz, feldspars, lithoclasts
13 and matrix content the rock is classified as quartz-arenite and some areas with higher matrix
14 content (ca. 15%) as medium grained quartz-wacke (Folk 1974; Pettijohn et al.1987).

15 The identified porosity is more abundant than in the samples before CO_2 injection. The
16 estimated visual percentage ranges from 12 to 18%. Adapting Choquette and Pray (1970) and
17 Lucía (1999) nomenclatures, there are various pore types present in the rock. Intercrystalline
18 pores between quartz grains with variable sizes (90-240 μm) were observed. The presence of
19 pores that are arranged in micro-fractures within quartz grains is also common. Cavern type
20 pores appear frequently, with irregular shapes and sizes varying from 700 to 1700 μm , up to
21 2900 μm . Sometimes they are interconnected by micro-channels. Caverns are generally larger
22 than in the sample before CO_2 injection. Sometimes, matrix rich bands show elongated
23 channel pores following the anisotropy with a maximum dimension of 4.8 mm. The SEM
24 studies (Figs. 5 b, d, and f) showed again intergranular spaces constituted by cavern pores
25 interconnected by micro-channels and pore spaces sometimes filled with minerals.
26 Furthermore, the high degree of fracturing leads to fracture type pore development.

27 The pore network quantification by OIA was developed, as previously described, on digital
28 images acquired using objective lens of 10x. The estimated porosity percentage ranges from
29 7.06 to 22.05% (Table 1), with an average of $13.42 \pm 0.17\%$. The maximum area of pore was
30 $250,000 \mu\text{m}^2$ and the minimum was $9 \mu\text{m}^2$. The average pore area size was $278 \mu\text{m}^2$. Curves
31 of relative and absolute distribution of number of pores versus pore area ranges and diagrams

1 of weighted area related to pore area classes are presented in Figs. 6b and d for the samples
2 after SC CO₂ injection.

3 **4.2 Chemical analysis**

4 The composition of the brine was analyzed before and after the 24h testing and the results are
5 shown in Table 2. The data of brine composition before and after experimental CO₂ injection
6 show that there were some changes in the chemistry (higher than the total uncertainty of the
7 technique: $\approx 10\%$): a decrease (ca. 30%) of the Ca²⁺, Mg²⁺ and SO₄²⁻ contents and an increase
8 on the HCO₃⁻ and NO₃⁻ contents. Other chemical parameters also decreased as a result of the
9 CO₂ injection: the pH changed from 7.2 to 5.27 and the conductivity also decreased around
10 12%.

11 Total rock analyses were performed on blocks with and without experimental CO₂-brine
12 exposure. The values and uncertainties are presented in Table 3. There were changes in the
13 following contents: increase of MgO (30%), Na₂O (20%) and CaO (ca. 200%). We
14 considered as significant a change over the uncertainties given by the laboratory for each
15 element, which uncertainty values range from 6.8 to 19.9% depending on the element. Two
16 samples were analysed by XRD, one previous to brine exposure and to SC CO₂ injection and
17 the other after the SC CO₂-brine experiment. These analyses only detected quartz, the other
18 phases being present in quantities below the detection limit of this technique. Furthermore,
19 the residue that remained in the chamber of the reactor after the experiment was studied (Fig.
20 7). This residue consisted mainly of quartz in two different fractions: a fine fraction with sizes
21 around 20 μ m and another fraction with rounded quartz grains sometimes reaching 1mm in
22 size.

23

24 **5 Discussion**

25 In the studied Utrillas sandstones, OpM and SEM techniques allowed us to detect qualitative
26 changes in the pore network in the samples before and after SC CO₂ injection. Compared to
27 the pre-experiment samples, we can point out that, in general, after the experiment larger
28 pores are more common (700-1800 μ m) and cavern type pores and channels dominate (Figs. 4
29 a-b and 5 a-b). There is also an increase of grain fracturing (Figs. 4c and d; Figs. 5c and d).
30 Moreover, the edges of quartz grains before the experiment contain angular pits (Fig. 5e),

1 while pits in quartz after the experiment are less numerous and distinctly rounded and
2 enlarged (Fig. 5f).

3 Quantification of these changes was systematically carried out applying OIA (Fig. 3). This
4 study reveals an increase of porosity (Δn) of 0.57-1.58-3.87% with an average of 2.01%
5 (Table 1), which value is higher than the uncertainty of the OIA technique ($\approx 1.25\%$)
6 (Demirmen, 1972; Grove and Jerram, 2011). The lower error of this method as compared to
7 others is one of the advantages of the OIA technique (e.g. error of point counting is around
8 2.5%; Chayes and Faibain, 1951; Grove and Jerram, 2011).

9 The OIA technique also allowed us a complete characterization of the pore network through
10 curves of relative and absolute distribution of the number of pores versus pore area ranges
11 (Fig. 6) and diagrams of weighted area related to pore area classes for samples before and
12 after SC CO₂ injection. The pore area ranges measured by OIA are between 9 μm^2 and
13 250,000 μm^2 . The distribution of data shows that $\approx 99\%$ of pores correspond to pores smaller
14 than 1250 μm^2 (Fig. 6a). In the CO₂ injected sample (Fig. 6b) these small pores represent \approx
15 98% of all the pores. The diagrams of the weighted area related to pore area classes before
16 (Fig. 6c) and after SC CO₂ injection (Fig. 6d) show that the contribution of the first class of
17 pore area is ca. 35% of the total porosity for pre-experiment samples and ca. 25% of the total
18 porosity for samples after the experiment. The approximate contributions of cumulative
19 weighted pore area for the main percentiles for the sample before SC CO₂ injection are: <
20 1,250 μm^2 (25%), 7,500 μm^2 (50%), and 38,750 μm^2 (75%). On the other hand, the sample
21 after injection shows contributions of 25% of pore area of 1,250 μm^2 , 50% of 8,750 μm^2 , and
22 75% of 65,000 μm^2 . In general, in the original samples there are more pores of smaller and
23 intermediate pore area classes than in the ones after the injection. Besides, the maximum sizes
24 of pore area are larger in the injected samples, **similarly, Tarkowski and Wdowin (2011)**
25 **described an increase in the mean pore diameters in their studies.**

26 The brine chemistry study showed that Na⁺, K⁺, Cl⁻ and SiO₂ values did not suffer any
27 relevant changes after the injection. On the other hand, the Ca²⁺, Mg²⁺ and SO₄²⁻ content
28 decreased by approx. 30% (Table 2), probably all as a result of local mineral precipitation of
29 Mg, Ca and Na minerals, evidenced by an increase of these oxides in the chemistry of the
30 rock after the experiment (Table 3). The brine chemistry data, in relative terms is similar to
31 those found in the literature (Kaszuba et al., 2005), but different to the analysis completed by
32 **Tarkowski and Wdowin 2011**; Luquot et al., 2012; Yu et al., 2012 and Wdowin et al., 2014a,

1 b. This is probably due to the initial composition of our samples, conditioned by the
2 chemically resistant quartz (95% wt.) and the short period of our experimentation (24 h). We
3 can say that preliminarily CO₂-brine contact with the rock initiated some mineral precipitation
4 though not to a relevant scale. It also caused brine pH reduction (changing from 7.2 to 5.2),
5 similarly to other cases (Kaszuba et al., 2005; Tarkowski and Wdowin, 2011). The pH
6 reduction is due to the increase of carbonic acid and NO₃⁻ content of the brine after the
7 experiment (Table 2). The higher amount of carbonic acid originates from the CO₂ dissolution
8 in the brine, while that of the NO₃⁻ may be due to reactions with organic material present in
9 the rock sample. The overall data of the total rock composition of before and after SC CO₂-
10 brine exposure do not show precipitation/dissolution of mineral phases. We can conclude that
11 that the reactions between minerals and fluids were not significant (Gunter et al., 1997 and
12 Hitchon, 1996) and the changes in the porosity configuration (Table 1) are due to physical
13 processes.

14 The observed and measured changes in the studied samples are due to the SC CO₂-brine
15 exposure and can be of importance in the vicinity of the injection well (Fig. 1a) where the
16 interaction of the CO₂ and the rock takes place initially in wet conditions (Kharaka et al.
17 2006; Gaus, 2010; André et al., 2007). Any modification in mineralogy and porosity (Figs. 4,
18 5 and Table 1) changing the rock texture could affect the injection well and its closest
19 environment and hence the injection efficiency (Wdowin et al., 2014a). Our experimental
20 investigation indicates that the main effects observed after the experiment are relevant to the
21 pore network characteristics and quantification, while changes regarding chemical
22 characteristics of the brine and total rock are minor. **The initial heterogeneity of the rock
23 could condition the comparison of physical and chemical parameters between the before and
24 after CO₂ injection tests samples, as described by Tarkowski and Wdowin (2011) and
25 Wdowin et al. (2014b). In our study we tried to minimize this effect studying rock surfaces
26 few millimetres separation and employing expert criteria in petrography.**

27 All these considerations allow us to build a conceptual model for the experimental SC CO₂
28 injection (Figs. 8a to d). The CO₂ input and release affected the quartz matrix and quartz
29 skeletal grains in different ways that finally lead to detachment and partial re-adjustment of
30 the quartz volume (except in the area with firmly fixed quartz grains or areas without CO₂-
31 brine access). These effects resulted in a partial loss of the quartz (both grains and matrix),
32 present as residue after the experiment (Fig. 7). Our conceptual model consists of four stages.

- 1 • Stage 1 (Fig. 8a): Initial mineralogical and textural conditions of the rock saturated with
2 brine. Quartz constitutes 95% of the rock sample and brine partially fills intergranular spaces.
- 3 • Stage 2 (Fig. 8b): pressurized SC CO₂ injection: initial CO₂ input would mix with brine
4 and percolate through the rock pore system generating a mechanical dragging force probably
5 opening/widening some of the inter quartz-particle cracks.
- 6 • Stage 3 (Fig. 8c): pressurized CO₂-brine stabilization: this stage extends through most of
7 the experimental run (24 h). During this time, SC CO₂ continues to diffuse into the pore
8 structure causing accommodation inside (small fractures) and between quartz grains,
9 producing instability in the rock cohesion.
- 10 • Stage 4 (Fig. 8d): CO₂-brine pressure release and expansion: Intra-quartz particle CO₂
11 expansion during pressure release would promote further internal quartz breakdown and
12 generation of free micro-quartz grains (Figs 4b, d and f; Figs. 5b, d and f). This pressure
13 release and gas and brine expansion generated outward dragging forces that probably
14 favoured partial loss of quartz grains that were collected in the chamber when the experiment
15 was finished. This would allow us to explain the porosity increase in the rock.

16 This model explains how the indirect mineralogical-compositional changes, (identified by
17 OpM, SEM Figs. 4 and 5), may be related to possible de-cohesion of the quartz matrix
18 possibly caused by CO₂-brine pressure (Fauria and Rempel, 2011; Berrezueta et al., 2013). If
19 the system is open, the de-cohesion causes part of the mineral phases of the matrix to leave
20 the system generating a mineralogical-compositional change. The nature of this change is
21 physical and not chemical. The possible de-cohesion of the matrix, by the action of CO₂, leads
22 logically to an increase in the porosity. Therefore, the observed increase in porosity is most
23 probably caused by this de-cohesion and matrix loss, in our experiments.

24

25 **6 Conclusions**

26 Quantitative assessment of petrography and mineralogy by OIA can be an important tool for
27 geosciences, providing numerical values as a key to the successful interpretation of the rock
28 texture and mineralogy.

29 The proposed methodology, consisting of mineralogical and petrographic studies by OpM,
30 SEM and OIA techniques on sandstones subjected to SC CO₂-brine exposure (7.8 MPa, 38°

1 C, during 24 h), proved to be highly effective for the identification and measurement of
2 changes in the pore network. For this study, the Utrillas sandstones were selected due to their
3 potential as CO₂ reservoir in Spain. However, the same methodology could be applicable for
4 future studies considering other rock types, different CO₂ storage conditions or longer periods
5 of exposure time.

6 The influence of the original rock composition and texture is very important and leads to
7 different effects of the SC CO₂-brine exposure. The study of potential changes at rock matrix
8 scale depends on the facies variations of any sedimentary formation, when evaluating a
9 possible CO₂ reservoir. The facies studied in this work is characterized by 95% quartz content
10 and heterogeneous rock texture, where micro-channels in the quartz matrix areas favour the
11 SC CO₂-brine injection resulting in the development of bigger cavities and pore channels. The
12 main pore evolution measured by OIA was an increase of porosity (2.10 %) and a
13 readjustment of pore network distribution regarding pore size classes.

14 The chemical analysis of whole rock and brine, before and after SC CO₂-brine injection, point
15 out the prevalence of physical processes with regard to chemical processes
16 (dissolution/precipitation) during the early injection phases. The chemical-compositional
17 evolution of the analysed elements did not evidence significant mineralogical processes.
18 Supercritical CO₂ causes brine pH to decrease as a consequence of carbonic acid increase,
19 validating published models about the effect of supercritical CO₂ on brine.

20 The results of this experiment show that the changes occurred due to physical process
21 allowing a rough approximation of the CO₂-brine-rock interactions. Furthermore, these
22 changes may have an important impact on the behaviour of reservoir rocks during first
23 injection phases of SC CO₂: i) changes in the rock system that lead to the porosity evolution
24 could facilitate further CO₂ injection, ii) mobilization of solid material (quartz) should be
25 considered during experiments and/or future modelling of the reservoir.

26

27 **Acknowledgements**

28 The authors would like to thank the funding provided through the ALGECO2-IRMC Project
29 (Instituto Geológico y Minero de España: 2294-2013), CO₂-Pore Project (Plan Nacional de
30 España: 2009-10934, FEDER-UE), Minería XXI Project (CYTED: 310RT0402) and DIA-
31 CO₂ Projects I and II (CIUDEN: ALM/09/032 and ALM/12/028). Thanks are due to Roberto

1 Martínez, Félix Mateos, Luís González-Menéndez, Isabel Suárez and Ricardo Molinero for
2 providing help in OIA techniques, SEM analysis, data acquisition, and statistical treatment for
3 rock sample collection and to Timea Kovacs for her suggestions.

4

5 **References**

- 6 Alonso, J.L., Pulgar, J.A., García-Ramos, J.C. and Barba, P. (1996). Tertiary basins and
7 Alpine tectonics in the Cantabrian Mountains (NW Spain). In: P.F. Friend and C.J. Dabrio
8 (eds), Tertiary basins of Spain: The stratigraphic record of crustal Kinematics, Cambridge
9 University Press, Cambridge, 214-227.
- 10 André, L., Audigane, P., Azaroual, M. and Menjoz, A. (2007). Numerical modelling of fluid-
11 rock chemical interactions at the supercritical CO₂-liquid interface during CO₂ injection into
12 a carbonate reservoir, the Dogger aquifer (Paris Basin, France). *Energy Conversion and*
13 *Management*, 48(6), 1782-1797.
- 14 Bacci, G., Korre, A. and Durucan, S. (2011). An experimental and numerical investigation
15 into the impact of dissolution/precipitation mechanisms on CO₂ injectivity in the wellbore
16 and far field regions. *International Journal of Greenhouse Gas Control*, 5(3), 579-588.
- 17 Bachu, S. (2000). Sequestration of CO₂ in geological media: criteria and approach for site
18 selection in response to climate change. *Energy Conversion and Management*, 41(9), 953-
19 970.
- 20 Benson, S. M. and Cole, D.R. (2008). CO₂ sequestration in deep sedimentary formations.
21 *Elements*, 4(5), 325-331.
- 22 Berrezueta, E., González-Menéndez, L., Breitner, D. and Luquot, L. (2013). Pore system
23 changes during experimental CO₂ injection into detritic rocks: Studies of potential storage
24 rocks from some sedimentary basins of Spain. *International Journal of Greenhouse Gas*
25 *Control*, 17, 411-422.
- 26 Berrezueta, E., González-Menéndez, L., Ordoñez-Casado, B. and Olaya, P. (2015). Pore
27 network quantification of sandstones under experimental CO₂ injection using Image
28 Analysis. *Computer and Geosciences*, 77, 97-110.
- 29 Bertier, P., Swennen, R., Laenen, B., Lagrou, D. and Dreesen, R., (2006). Experimental
30 identification of CO₂-water-rock interactions caused by sequestration of CO₂ in Westphalian

1 and Buntsandstein sandstones of the Campine Basin (NE-Belgium). *Journal of Geochemical*
2 *Exploration*, 89(1), 10-14.

3 Burton, M., Kumar, K. and Bryant, S.L., (2008). Time-dependent injectivity during CO₂
4 storage in aquifers. In *Symposium on Improved Oil Recovery Tulsa, Okla. Proceedings:*
5 *Richardson, Tex., Society of Petroleum Engineers*, paper SPE 113937, p. 15.

6 Cailly, B., Le Thiez, P., Egermann, P., Audibert, A., Vidal-Gilbert, S. And Longaygue, X.
7 (2005). Geological storage of CO₂: A state-of-the-art of injection processes and technologies.
8 *Oil & gas science and technology*, 60(3), 517-525.

9 Chayes, F. and Fairbairn, H. W. (1951). A test of the precision of thin-section analysis by
10 point counter. *American Mineralogist*, 36, 704-712.

11 Choquette, P.W. and Pray, L.C. (1970). Geologic nomenclature and classification of porosity
12 in sedimentary carbonates. *AAPG bulletin*, 54(2), 207-250.

13 Demirmen, F. (1972). Operator error in petrographic point-count analysis: a theoretical
14 approach. *Journal of the International Association for Mathematical Geology*, 4(1), 35-43.

15 Desbois, G., Urai, J.L., Kukla, P.A., Konstanty, J. and Baerle, C. (2011). High-resolution 3D
16 fabric and porosity model in a tight gas sandstone reservoir: a new approach to investigate
17 microstructures from mm-to nm-scale combining argon beam cross-sectioning and SEM
18 imaging. *Journal of Petroleum Science and Engineering*, 78(2), 243-257.

19 Egermann, P., Bazin, B. and Vizika, O. (2005). An experimental investigation of reaction-
20 transport phenomena during CO₂ injection. In *SPE Middle East Oil and Gas Show and*
21 *Conference. Society of Petroleum Engineers*.

22 Evers, H.J. (1967). Geology of the Leonies between the Bernesga and Porma rivers,
23 Cantabrian Mountains, NW Spain. *Leidse Geol. Meded.*, 41, 83-151.

24 Fauria, K.E. and Rempel, A.W. (2011). Gas invasion into water-saturated, unconsolidated
25 porous media: Implications for gas hydrate reservoirs. *Earth and Planetary Science Letters*,
26 312(1), 188-193.

27 Fischer, S., Liebscher, A., De Lucia, M. and Hecht, L. (2013). Reactivity of sandstone and
28 siltstone samples from the Ketzin pilot CO₂ storage site-Laboratory experiments and reactive
29 geochemical modeling. *Environmental earth sciences*, 70(8), 3687-3708.

30 Folk, R. L., (1974). *Petrology of Sedimentary Rocks*. Hemphill's, Austin, Texas, 170 pp.

1 Gallastegui, J. (2000). Estructura cortical de la Cordillera y Margen Continental Cantábricos:
2 Perfiles ESCI-N. Trabajos de Geología, Universidad de Oviedo, 22, 9-234.

3 García Lobón, J.L., Reguera García, M.I, Martín León, J., Rey Moral, C. and Berrezueta, E.
4 (2010). Plan de selección y caracterización de áreas y estructuras favorables para el
5 almacenamiento geológico de CO₂ en España. Resumen ejecutivo Instituto Geológico y
6 Minero de España (IGME), Madrid.

7 Gaus, I. (2010). Role and impact of CO₂-rock interactions during CO₂ storage in sedimentary
8 rocks. *International Journal of Greenhouse Gas Control*, 4(1), 73-89.

9 Gaus, I., Audigane, P., Andre, L., Lions, J., Jacquement, N., Durst, P., Czernichowski, I. and
10 Azaroual, M., (2008). Geochemical and solute transport modelling for CO₂ storage, what to
11 expect from it?. *International Journal of Greenhouse Gas Control*, 2(4), 605-625.

12 Grove, C. and Jerram, D.A. (2011). jPOR: An ImageJ macro to quantify total optical porosity
13 from blue-stained thin sections. *Computers & Geosciences*, 37(11), 1850-1859.

14 Gunter, W.D., Wiwehar, B. and Perkins, E.H. (1997). Aquifer disposal of CO₂-rich
15 greenhouse gases: extension of the time scale of experiment for CO₂-sequestering reactions
16 by geochemical modelling. *Mineralogy and Petrology*, 59(1-2), 121-140.

17 Gunter, W.D., Bachu, S. and Benson, S. (2004). The role of hydrogeological and geochemical
18 trapping in sedimentary basins for secure geological storage of carbon dioxide. *Geological*
19 *Society, London, Special Publications*, 233(1), 129-145.

20 HEL user's guide (5.1) for Windows, (2009). WinISO Software control System Reactor.

21 Hitchon, B. (1996). Aquifer disposal of carbon dioxide: hydrodynamic and mineral trapping-
22 proof of concept. Geoscience Publishing Ltd, Alberta, Canada, 165pp.

23 Holloway, S. (1997). An overview of the underground disposal of carbon dioxide. *Energy*
24 *Conversion and Management*, 38, S193-S198.

25 IMAGE-PRO® R PLUS user's guide (7.0) for Windows, 2009. Software Program of Media
26 Cybernetics. Inc.

27 Izgec, O., Demiral, B., Bertin, H.J. and Akin, S. (2005). Experimental and numerical
28 investigation of carbon sequestration in saline aquifers. In SPE/EPA/DOE Exploration and
29 Production Environmental Conference. Society of Petroleum Engineers.

1 Izgec, O., Demiral, B., Bertin, H.J. and Akin, S. (2008). CO₂ injection into saline carbonate
2 aquifer formations I: laboratory investigation. *Transport in Porous Media*, 72(1), 1-24.

3 Kharaka, Y.K., Cole, D.R., Hovorka, S.D., Gunter, W.D., Knauss, K.G. and Freifeld, B.M.
4 (2006). Gas-water-rock interactions in Frio Formation following CO₂ injection: Implications
5 for the storage of greenhouse gases in sedimentary basins. *Geology*, 34(7), 577-580.

6 Kaszuba, J.P., Janecky, D.R. and Snow, M.G. (2003). Carbon dioxide reaction processes in a
7 model brine aquifer at 200° C and 200 bars: implications for geologic sequestration of carbon.
8 *Applied Geochemistry*, 18(7), 1065-1080.

9 Kaszuba, J.P., Janecky, D.R. and Snow, M.G. (2005). Experimental evaluation of mixed fluid
10 reactions between supercritical carbon dioxide and NaCl brine: Relevance to the integrity of a
11 geologic carbon repository. *Chemical Geology*, 217(3), 277-293.

12 Ketzer, J.M., Iglesias, R., Einloft, S., Dullius, J., Ligabue, R. and De Lima, V. (2009). Water-
13 rock-CO₂ interactions in saline aquifers aimed for carbon dioxide storage: experimental and
14 numerical modeling studies of the Rio Bonito Formation (Permian), southern Brazil. *Applied*
15 *Geochemistry*, 24(5), 760-767.

16 Lake, L. W. (1989). Enhanced oil recovery. Pentice Hall. Englewood Cliffs, NJ.

17 Liu, H., Hou, M.Z., Gou, Y. and Were, P. (2013). Simulation of CO₂-Water-Rock Interaction
18 Processes-Mineral Scaling Problems in Saline Formations. In *Clean energy systems in the*
19 *subsurface: production, storage and conversion*. Springer Series in Geomechanics and
20 *Geoengineering*, 233-248.

21 Lobato, L., García-Alcalde, J.L., Sánchez de Posada, L.C., Truyols, J. and Servicio Geológico
22 S.A.H.V.L. (Cuenca Ciñera-Matallana) (1985). Mapa geológico de España a E. 1:50.000,
23 núm. 104 “Boñar”. Segunda Serie, Primera Edición. Instituto Geológico y Minero de España
24 (IGME), Madrid.

25 Lucia, F.J. (1999), Carbonate reservoir characterization: Berlin, Springer-Verlag, 226 p.

26 Luquot, L. and Gouze, P. (2009). Experimental determination of porosity and permeability
27 changes induced by injection of CO₂ into carbonate rocks. *Chemical Geology*, 265(1), 148-
28 159.

- 1 Luquot, L., Andreani, M., Gouze, P. and Camps, P. (2012). CO₂ percolation experiment
2 through chlorite/zeolite-rich sandstone (Pretty Hill Formation-Otway Basin-Australia).
3 *Chemical geology*, 294, 75-88.
- 4 Manjón Rubio, M., Vargas Alonso, I., Colmenero Navarro, J.R., García-Ramos, J.C.,
5 Gutiérrez Elorza, M. and Molina, E. (1982a). Memoria del Mapa geológico de España E.
6 1:50.000, Hoja núm. 130 (Vegas del Condado). Segunda Serie, Primera Edición. Instituto
7 Geológico y Minero de España (IGME), Madrid.
- 8 Manjón Rubio, M., Vargas Alonso, I., Colmenero Navarro, J.R., García-Ramos, J.C., Crespo
9 Zamorano, A. and Matas González, J. (1982b). Mapa geológico de España E. 1:50.000, Hoja
10 núm. 130 (Vegas del Condado). Segunda Serie, Primera Edición. Instituto Geológico y
11 Minero de España (IGME), Madrid.
- 12 Martínez, R., Suarez, I., Carneiro, J., Zarhloule, Y., Le Nindre, Y. and Boavida, D. (2013).
13 Storage capacity evaluation for development of CO₂ infrastructure in the west Mediterranean.
14 *Energy Procedia*, 37, 5209-5219.
- 15 Mito, S., Xue, Z. and Ohsumi, T. (2008). Case study of geochemical reactions at the Nagaoka
16 CO₂ injection site, Japan. *International Journal of Greenhouse Gas Control*, 2(3), 309-318.
- 17 Olivé Davó, A., Álvaro López, M., Ramírez del Pozo, J. and Aguilar Tomás, M. (1989).
18 Memoria del Mapa Geológico de España a Escala 1:200.000, Hojas N° 5/12 (Bermeo/Bilbao).
19 Instituto Tecnológico Geominero de España, Madrid, 208 pp.
- 20 Perkins, E.H. and Gunter, W.D. (1995). Aquifer disposal of CO₂-rich greenhouse gasses:
21 modelling of water-rock reaction paths in a siliciclastic aquifer. In: Kharaka, Y.K., Chidaev,
22 O.V. (Eds.), *Water-rock Interactions*, Brookfield, Rotterdam, 895-898.
- 23 Pettijohn, F.J., Potter, P.E. and Siever, R., (1987). *Sand and Sandstones*. Springer, Berlin, 553
24 pp.
- 25 Quintana, L., Pulgar, J.A. and Alonso, J.L. (2015). Displacement transfer from borders to
26 interior of a plate: a crustal transect of Iberia. *Tectonophysics*.
- 27 Rochelle, C.A., Czernichowski-Lauriol, I. and Milodowski, A.E. (2004). The impact of
28 chemical reactions on CO₂ storage in geological formations: a brief review. *Geological*
29 *Society, London, Special Publications*, 233(1), 87-106.

- 1 Rosenbauer, R.J., Koksalan, T. and Palandri, J.L. (2005). Experimental investigation of CO₂-
2 brine-rock interactions at elevated temperature and pressure: implications for CO₂
3 sequestration in deep-saline aquifers. *Fuel Processing Technology*, 86(14), 1581-1597.
- 4 Ross, G.D., Todd, A.C., Tweedie, J.A. and Will, A.G. (1982). The Dissolution Effects of
5 CO₂-Brine Systems on the Permeability of UK and North Sea Calcareous Sandstones. In
6 SPE/DOE 10685 Enhanced Oil Recovery Symposium. Society of Petroleum Engineers.
- 7 Rupke, J. (1965). The Esla Nappe, Cantabrian Mountains (Spain). *Leidse Geol. Meded.* 32, 1-
8 74, 34 fig., 6 láms. Leiden.
- 9 Saeedi, A., Rezaee, R., Evans, B. and Clennell, B. (2011). Multiphase flow behaviour during
10 CO₂ geo-sequestration: Emphasis on the effect of cyclic CO₂-brine flooding. *Journal of*
11 *Petroleum Science and Engineering*, 79(3), 65-85.
- 12 Sayegh, S.G., Krause, F.F., Girard, M. and DeBree, C. (1990). Rock/fluid interactions of
13 carbonated brines in a sandstone reservoir: Pembina Cardium, Alberta, Canada. *SPE*
14 *Formation Evaluation*, 5(04), 399-405.
- 15 Span, R. and Wagner, W. (1996). A new equation of state for carbon dioxide covering the
16 fluid region from the triple-point temperature to 1100 K at pressures up to 800 MPa. *Journal*
17 *of physical and chemical reference data*, 25(6), 1509-1596.
- 18 Sterpenich, J., Sausse, J., Pironon, J., Géhin, A., Hubert, G., Perfetti, E. and Grgic, D. (2009).
19 Experimental ageing of oolitic limestones under CO₂ storage conditions: Petrographical and
20 chemical evidence. *Chemical geology*, 265(1), 99-112.
- 21 Svec, R.K. and Grigg, R.B. (2001). Physical effects of WAG fluids on carbonate core plugs.
22 In SPE 71496 Annual Technical Conference and Exhibition. Society of Petroleum Engineers.
- 23 Tarkowski, R. and Wdowin, M. (2011). Petrophysical and mineralogical research on the
24 influence of CO₂ injection on Mesozoic reservoir and caprocks from the polish lowlands. *Oil*
25 *& Gas Science and Technology–Revue d'IFP Energies nouvelles*, 66(1), 137-150.
- 26 Tarkowski, R., Wdowin, M. and Manecki, M. (2015). Petrophysical examination of CO₂-
27 brine-rock interactions-results of the first stage of long-term experiments in the potential
28 Zaosie Anticline reservoir (central Poland) for CO₂ storage. *Environmental monitoring and*
29 *assessment*, 187(1), 1-10.
- 30 Trujols, J., Álvarez, F., Arbizu, M.A., García-Alcalde, J.L., García-López, S., Martínez-

- 1 Chacón, M.L., Méndez Bedia, I., Méndez-Fernández, C.A., Menéndez, J.R., Sánchez de
2 Posada, L., Sotos, F., Lobato, L. and Rodríguez Fernández, L.R. (1984). Memoria del Mapa
3 geológico de España E. 1:50.000, Hoja núm. 104 (Boñar). Segunda Serie, Primera Edición.
4 Instituto Geológico y Minero de España (IGME), Madrid.
- 5 Vickerd, M.A., Thring, R.W., Arocena, J.M., Li, J.B. and Heck, R.J. (2006). Changes in
6 porosity due to acid gas injection as determined by X-ray computed tomography. Journal of
7 Can. Petrol. Technol., 45(08), 6 pp.
- 8 Wdowin, M., Tarkowski, R. and Franus, W. (2014a). Determination of changes in the
9 reservoir and cap rocks of the Chabowo Anticline caused by CO₂-brine-rock interactions.
10 International Journal of Coal Geology, 130, 79-88.
- 11 **Wdowin, M., Tarkowski, R., and Franus, W. (2014b). Supplementary Studies of Textural and**
12 **Mineralogical Changes in Reservoir and Caprocks from Selected Potential Sites Suitable for**
13 **Underground CO₂ Storage. Arabian Journal for Science and Engineering, 39(1), 295-309.**
- 14 Yu, Z; Liu, L., Yang, S., Li, S. and Yang, Y. (2012). An experimental study of CO₂-brine-
15 rock interaction at in situ pressure-temperature reservoir conditions. Chemical Geology, 326-
16 327, 88-101.
- 17
- 18

1 **Table 1.** Total porosity of Utrillas sandstones (3 samples), before and after SC CO₂-brine
 2 exposure, measured by Optical Image Analysis (OIA). Average % is the average porosity of
 3 the 3 samples. *Uncertainly (1.25%) given by Oviedo- IGME Laboratory. Difference % is
 4 calculated as the variation in porosity % before and after CO₂-brine injection. Total Average
 5 % is the average of the differences between Porosity % before and after CO₂-brine injection.

6

	Before SC CO ₂ -brine		After SC CO ₂ -brine		Porosity variation		Interpretation
	Porosity %	Average %*	Porosity %	Average %*	Difference %	Total Average %	
Sample 1	18.18		22.05		3.87		
Sample 2	9.55	11.41±0.14	11.13	13.42±0.17	1.58	2.01	Increase
Sample 3	6.49		7.06		0.57		

7

8 **Table 2.** Chemical composition of natural brine before and after the experiment. *Uncertainty
 9 (10%) given by Madrid-IGME Laboratory (Water Analysis).

10

	Rock before CO ₂ and brine (mg/L) *	Rock after CO ₂ and brine (mg/L) *	Interpretation
Na ⁺	2378 ± 237.80	2351 ± 235.10	No change
K ⁺	139 ± 13.90	114 ± 11.40	No change
Ca ²⁺	570 ± 57.00	440 ± 44.00	Decrease: 30% (Δ = 130 mg/L)
Mg ²⁺	268 ± 26.80	200 ± 20.00	Decrease: 34% (Δ = 68 mg/L)
Cl ⁻	5200 ± 520	4640 ± 464.00	No change
SO ₄ ²⁻	624 ± 62.40	464 ± 46.40	Decrease: 34% (Δ = 160 mg/L)
HCO ₃ ⁻	14 ± 1.40	36 ± 3.60	Increase: 157% (Δ = 22 mg/L)
NO ₃ ⁻	1.1 ± 0.11	10 ± 0.10	Increase: 809% (Δ = 8.9 mg/L)
SiO ₂	9.3 ± 0.93	8.3 ± 0.83	No change
pH	7.2 (pH. Unit.)	5.27 (pH. Unit.)	Decrease: 36% (Δ = 1.93)
Conductivity	15350 (μS/cm)	13650 (μS/cm)	Decrease: 20% (Δ = 1700 μS/cm)

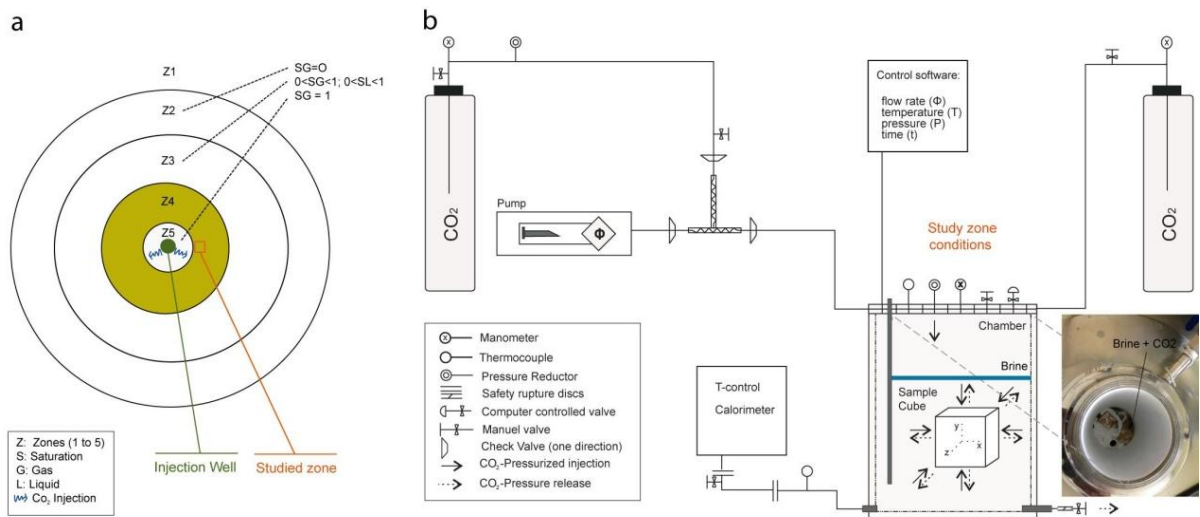
1

2 **Table 3.** Chemical composition of whole rock (Utrillas sandstone) before and after the
 3 experiment. Uncertainty given by IGME Laboratory (XRF Analysis).

4

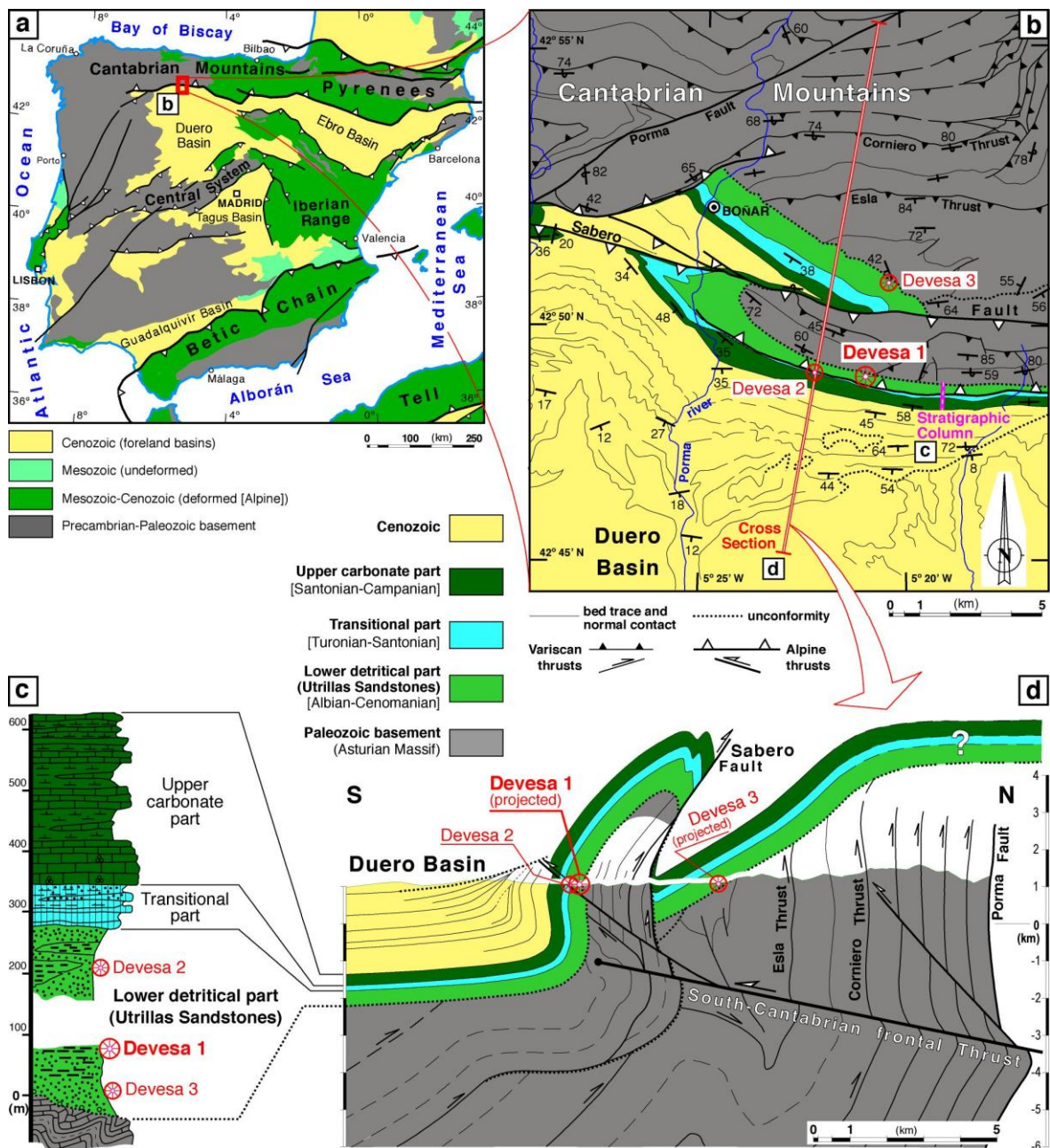
	Uncertainty (%)	Rock before CO ₂ and brine (%)	Rock after CO ₂ and brine (%)	Interpretation
SiO ₂	8.20	97.15 ± 2.5260	96.81 ± 2.5430	No change
Al ₂ O ₃	11.57	0.98 ± 0.1135	1.12 ± 0.1300	No change
Fe ₂ O ₃	9.55	0.30 ± 0.0290	0.28 ± 0.0270	No change
MnO	9.31	0	0	No change
MgO	7.96	0.03 ± 0.0025	0.04 ± 0.0030	Increase: 33% (Δ = 0.01 mg/L)
CaO	6.80	0.04 ± 0.0030	0.12 ± 0.0080	Increase:200%(Δ = 0.08 mg/L)
Na ₂ O	8.20	0.05 ± 0.0040	0.06 ± 0.0050	Increase: 20% (Δ = 0.01 mg/L)
K ₂ O	19.94	0.08 ± 0.0160	0.08 ± 0.0160	No change
TiO ₂	8.37	0.03 ± 0.0025	0.03 ± 0.0025	No change
P ₂ O ₅	10.95	0.01 ± 0.0010	0.01 ± 0.0010	No change
LOI	12.00	0.48 ± 0.0540	0.64 ± 0.0770	Increase: 33% (Δ = 0.16 mg/L)
TOTAL		99.16	99.20	

5

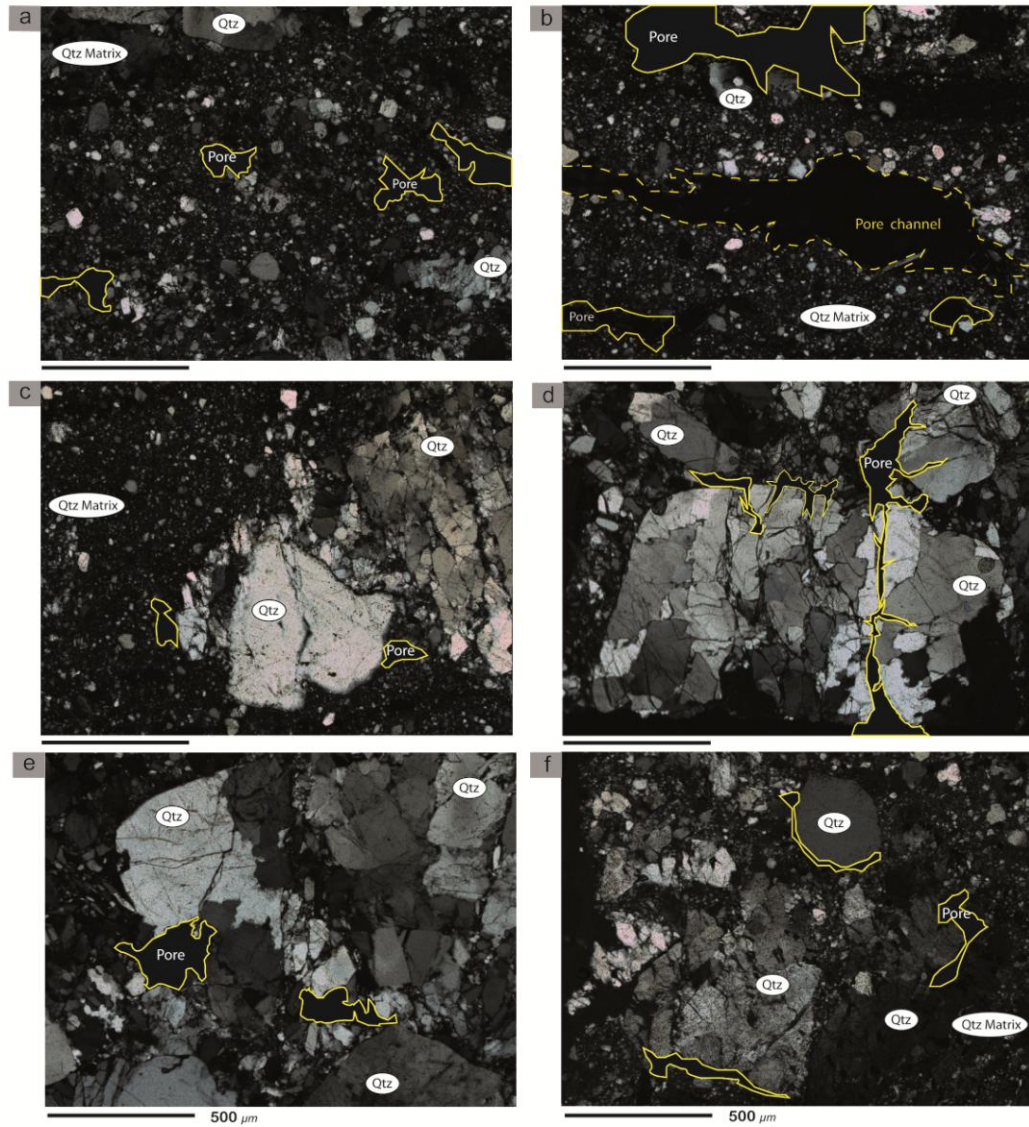


1
2
3
4
5
6
7
8
9
10
11

Figure 1. (a) Conceptual diagram of the reactive zones (Z1, Z2, Z3, Z4 and Z5) around the injection well according to André et al., 2007 and Gaus et al., 2008. Zone 1: Zone not affected by CO₂ injection; Zone 2: Acidified zone with dissolution and precipitation of minerals. Zone 3: Dissolution and precipitation of minerals (e.g. calcite and dolomite) and highly buffered pH. Zone 4: Highly saline water and salt precipitation (e.g. NaCl and MgSO₄). Zone 5: Dehydration reactions in open systems. (b) Layout of the experimental setup. Reactor system used for the pressurized CO₂ injection (modified from Berrezueta et al., 2013).

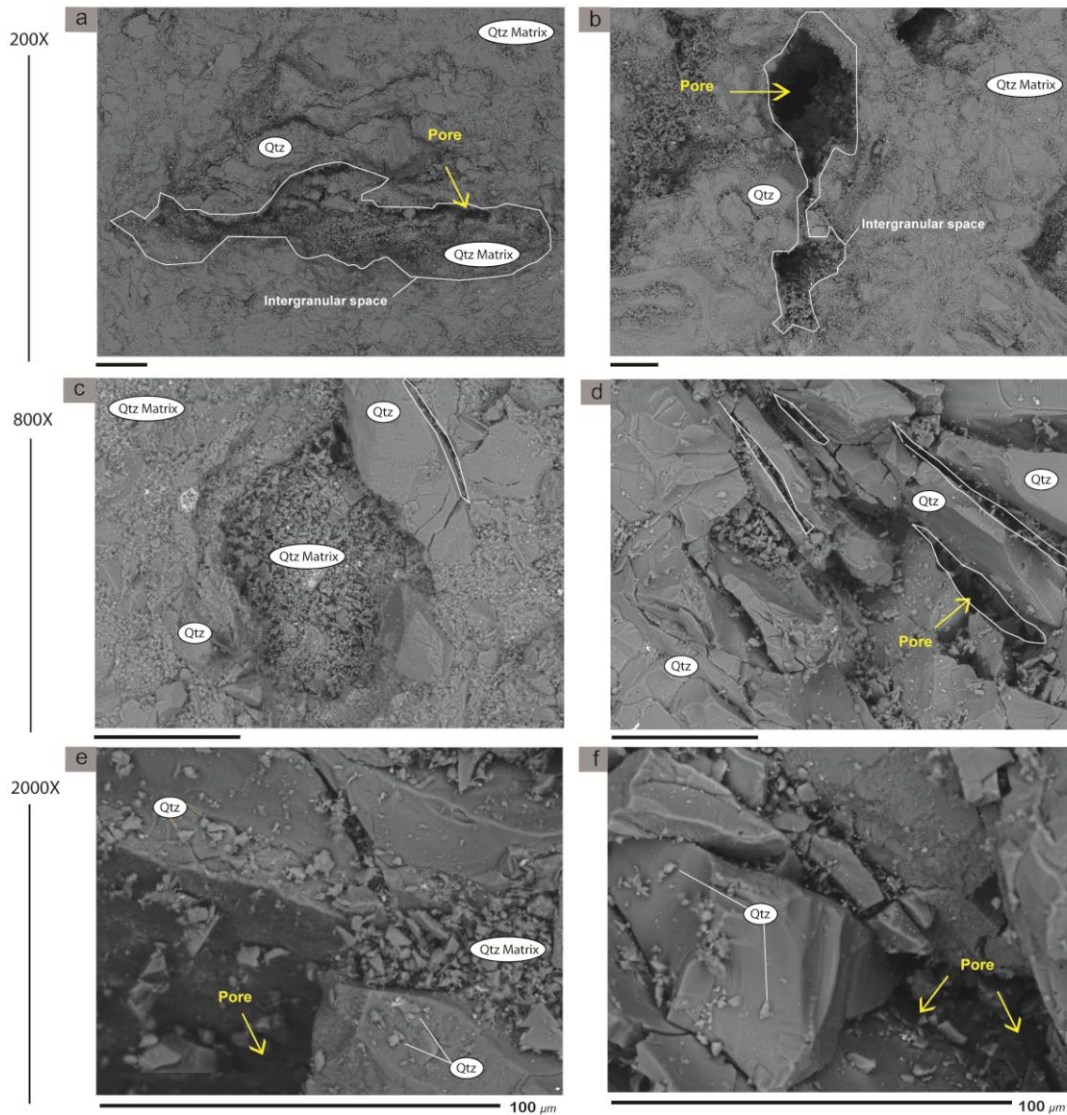


1
2
3 **Figure 2.** a) Location of the studied area in North Spain; modified from Quintana et al.
4 (submitted) b) Geological map and location of the sampling areas modified from Lobato et al.
5 (1985), Manjón Rubio et al. (1982b) and Alonso et al. (1996). c) Stratigraphic column of the
6 Cretaceous succession of the studied area. Location in “b”. Manjón Rubio et al. (1982b). d)
7 Geological cross-section along the sampling areas: boundary between the Cantabrian
8 Mountains and the Duero Basin. The geometry of the South Cantabrian frontal thrust and of
9 the Cenozoic materials of the Duero Basin taken from Alonso et al. (1996). Location in “b”.



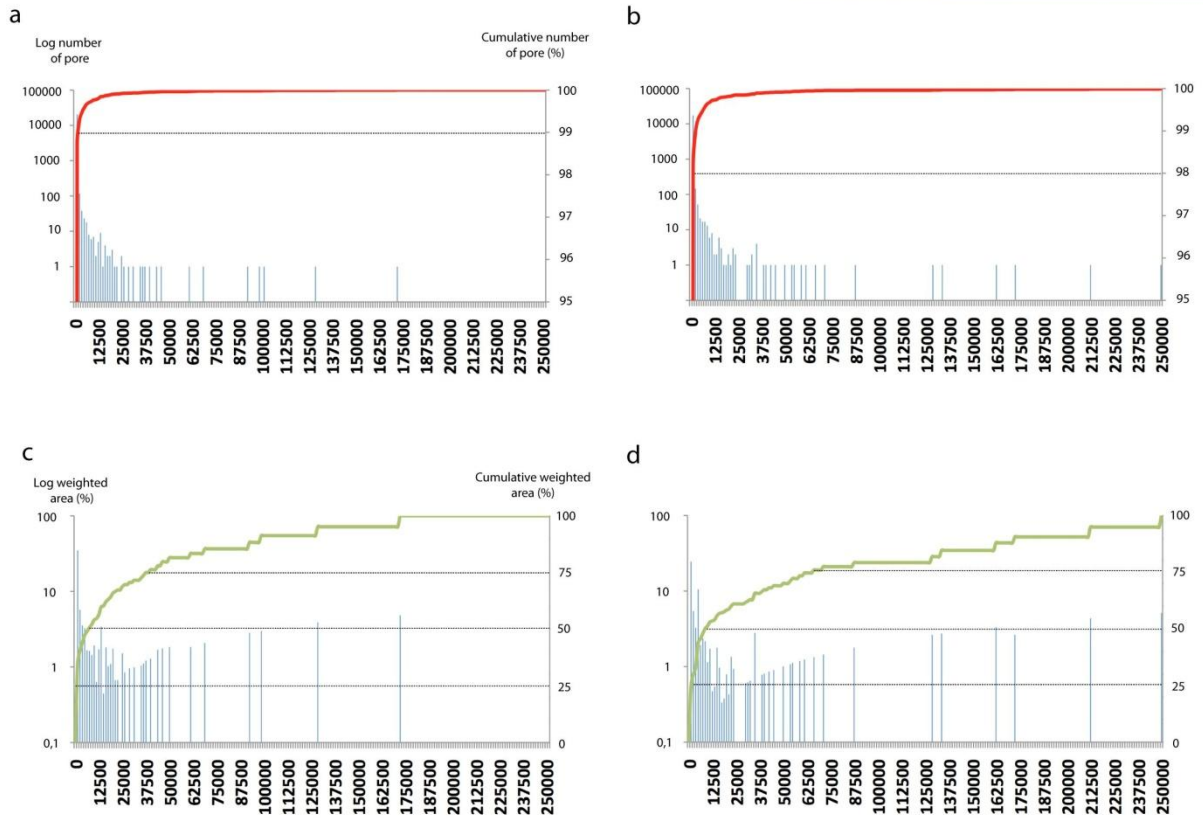
1
2

3 **Figure 4.** Textural and mineralogical characterization of the Utrillas sandstones. Optical
4 microscopy images obtained under cross-polarized light conditions acquired using objective
5 lens of 10x. Left images (a, c and e) correspond to samples before SC CO₂ injection; showing
6 the main textural and mineralogical features corresponding to quartz grains and sandy matrix
7 and intercrystalline pores within the matrix or in the vicinity of skeletal quartz grains. Right
8 images (b, d and f) correspond to samples after SC CO₂ injection; showing no changes in the
9 mineralogical features and a pore network characterized by the presence of channels, caverns
10 and pores within large quartz grains.



1
2

3 **Figure 5.** Secondary electron SEM micrographs of the Utrillas sandstones. Left images (a, c
4 and e) correspond to samples before SC CO₂ injection. Right images (b, d and f) correspond
5 to samples after SC CO₂ injection. a) Intergranular space filled with minerals; b) intergranular
6 spaces constituted by cavern pores interconnected by micro-channels with pore spaces
7 sometimes filled with minerals; c) intercrystalline space; d) high degree of fracturation of
8 quartz grains; e) the edges of quartz grains in the starting material (before CO₂-brine
9 exposure) contain angular pits; f) pits in quartz from the experiment are less numerous and
10 distinctly rounded and enlarged.

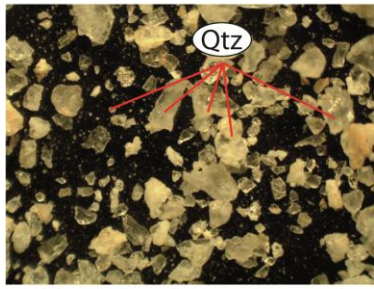


1

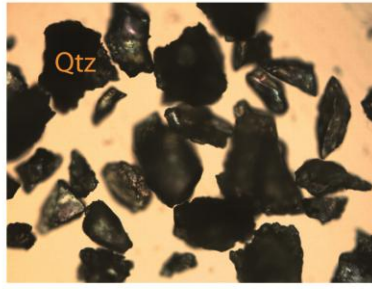
2

3 **Figure 6.** (a) X-axis vs left Y-axis: frequency diagrams of number of pores (Log scale) related
 4 to pore area classes (μm^2) before CO₂ injection (blue bars). X-axis vs right Y-axis: cumulative
 5 number of pores (%) related to pore area (μm^2) (red symbols). Red dashed line represents the
 6 contribution of the first class of pore area. (b) X-axis vs left Y-axis: frequency diagrams of
 7 weighted pore area (Log scale) related to pore area (μm^2) after CO₂ injection (blue bars). X-
 8 axis vs right Y-axis: cumulative weighted pore area (%) related to pore area classes (μm^2)
 9 (green symbols). Black dashed lines represent percentiles 25, 50, 75. c) X-axis vs left Y-axis:
 10 frequency diagrams of number of pores (Log scale) related to pore area (μm^2) before CO₂
 11 injection (blue bars). X-axis vs right Y-axis: cumulative number of pores (%) related to pore
 12 area (μm^2) (red symbols). Red dashed line represents the contribution of the first class to pore
 13 area. d) x vs left y axis: frequency diagrams of weighted pore area (Log scale) related to pore
 14 area (μm^2) after CO₂ injection (blue bars). X-axis vs right Y-axis: cumulative weighted pore
 15 area (%) related to pore area classes (μm^2) (green symbols). Black dashed lines represent
 16 percentiles 25, 50, 75. Minimum pore size considered in the study is $> 9 \mu\text{m}^2$.

Binocular (4 X)
Reflected light



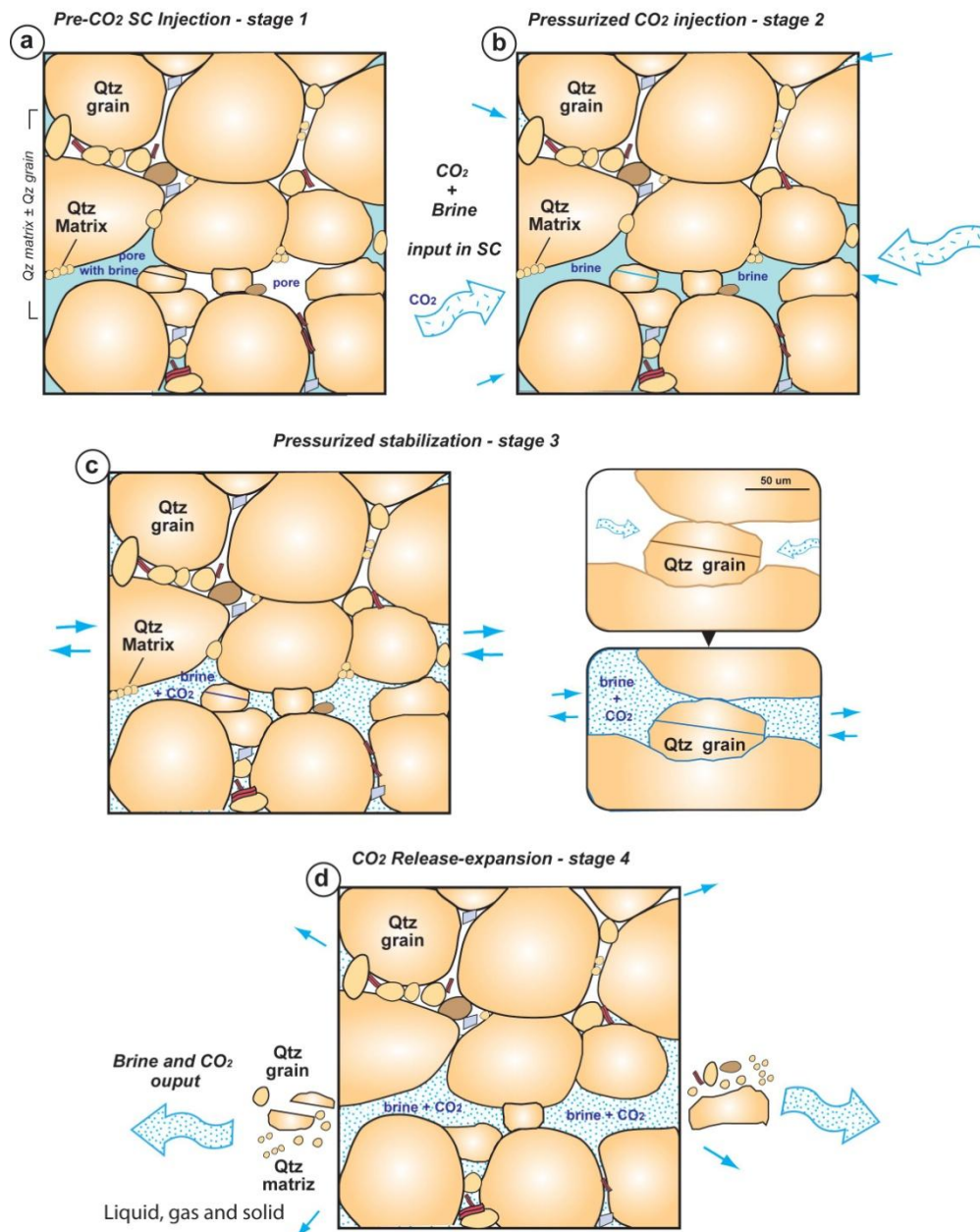
OpM (10 X)
Transmitted and Reflected Light



1

2 **Figure 7.** Photomicrographs by binocular microscope (reflected light) and by optical
3 microscope (transmitted and reflected light) of the residue that remained in the reactor
4 chamber after the experiment.

5



1
 2 **Figure 8.** Scheme of the model developed from the observed mineralogical/textural changes
 3 after the SC CO₂ injection in the Utrillas sandstones. As a summary: (a) initial mineralogy
 4 and texture of the sandstones: quartz is the 95% of the rock sample and brine partially fills
 5 some intergranular spaces. b) When the pressurized SC CO₂ injection begins, the injected gas
 6 fills the pore network (pores filled with brine and empty pores). c) During supercritical
 7 experimental stage, the pressurized CO₂ and brine is accommodated inside quartz grains
 8 (small fractures) and in the contacts between quartz, producing instability in the original rock
 9 cohesion. d) When the pressure releases, at the end stage of the experiment, CO₂ and brine
 10 expands generating more instability inside the sample, provoking an outwards drag force that
 11 causes leaks and may explain the observed quartz loss in the samples after the experiment.